Supplementary information

Supporting Online Material for
Observational evidence for volcanic impact on sea level and the global water cycle
A. Grinsted*, J. C. Moore, and S. Jevrejeva

*To whom correspondence should be addressed.
E-mail: ag@glaciology.net

This PDF file includes:
Methods and additional text
Supplementary Figs. 6 to 14
Supplementary Tables 1-4
Additional References

Supplementary Methods 1: Outlier removal

Prior to stacking the sea level rates from the individual tide gauges, outliers that may have been affected by earth-quake related vertical land movement were removed using a statistical scheme (see details in main paper). The statistics for these pre-processing steps are shown in Supplementary Table 1.

Supplementary Table 1: Virtual station pre-processing statistics.

Region	Outlier rates removed	Stations removed: skewness>.8	No. Stations remaining	Rates in final series	No rates filled by interp.
Antarctic	0	0	3	787	113
Arctic	2069	3	91	36225	2067
Baltic (excl.)	3120	0	75	52616	1024
CPacific	570	0	36	12764	846
Indian	1692	1	85	18651	1770
Mediterr	2543	4	78	18912	1555
NEAtlantic	5766	3	143	46061	2536
NEPacific	3734	2	95	33899	1592
NWAtlantic	3663	1	106	38402	1841
SEPacific	263	0	10	2709	156
SEAtlantic	67	0	9	1962	223
SWAtlantic	492	0	28	7674	624
WPacific	1140	1	147	44321	1759
Total (excl baltic)	**21999**	**15**	**831**	**262367**	**15082**

Supplementary Methods 2: Traditional estimates of confidence intervals.

The standard error on the median derived from N independent values with standard deviation σ (see Supplementary Figure 6) can traditionally be calculated as $1.253\sigma/\sqrt{N}$. Hence, a traditional estimate of the standard error of the median sea level in one and two year windows would be $1.253*5.8/\sqrt{(12*5)} = 0.93$mm and $1.253*5.8/\sqrt{(12*5*2)} = 0.66$ mm respectively. The standard error on the median difference will be $\sqrt{(\sigma_1^2+\sigma_2^2)}$, where σ_1 and σ_2 are the standard errors on the two medians, assuming independence of errors. For median difference between the 'Before' and 'Rise' windows we get a traditional estimate of the standard error of 1.1 mm, indicating that the observed difference of 8 mm is highly significant. However, the detrended sea level curve shows considerable auto-correlation and the assumption of independence is not valid in the equations for the standard error in the median and the standard error of the difference between medians. This leads to a gross overestimation of the significance using traditional methods. We therefore use robust bootstrap methods for dependent data (see methods section of main manuscript).

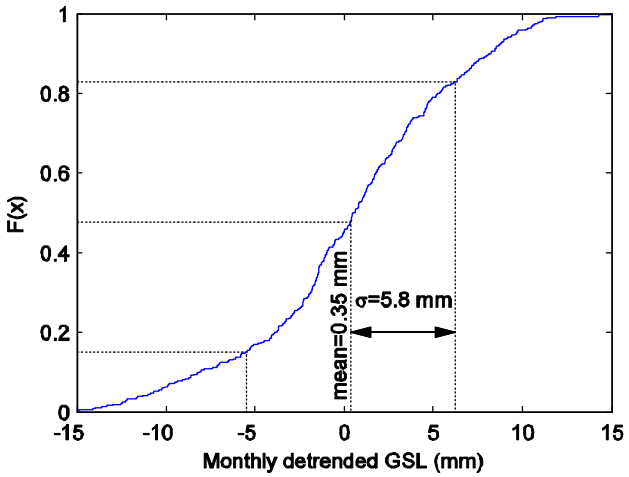

Supplementary Figure 6: The empirical cumulative distribution function (CDF) of the pre-eruption monthly detrended GSL from the 5 major eruptions. The mean is 0.35 mm and the standard deviation is 5.8 mm.

Supplementary Methods 3: Validation of Bootstrap error estimates.

The results presented in this paper depend critically on getting the statistics correct. Naïve bootstrap methods assume that the data is independent, which is rarely the case for time series. Some authors caution against using bootstrap methods on dependent (or auto-correlated) data as these methods often have not been sufficiently validated (34). In this section we show that the bootstrap scheme we devised performs excellently on time series with known characteristics that mimic real sea level variations quite closely.

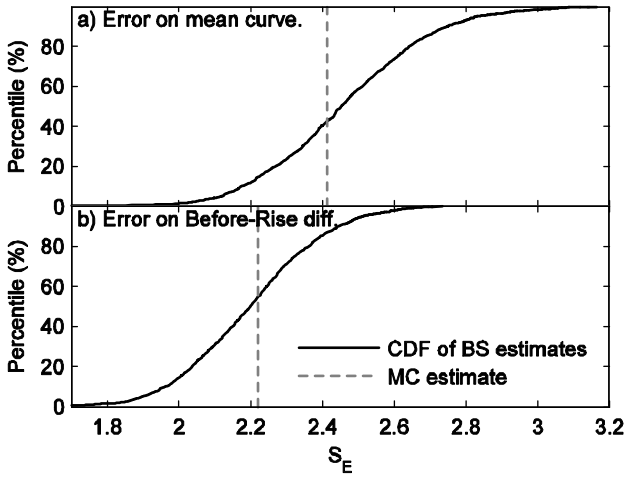

Supplementary Figure 7: Comparison of the standard errors estimated using the Bootstrap method (BS) with those obtained from Monte Carlo (MC) in the absence of any volcanic signal. a) shows the standard error on the mean curve and b) shows the standard error on the difference in means between the Before and Rise windows. The expected value of any particular BS error estimate is the 50% percentile value of S_E

We can test the performance of the bootstrap (BS) inferential scheme on realizations of a known parametric noise process. In contrast to real-world sea level time series, we do know the parameters of this process and can therefore estimate the errors to arbitrary precision using Monte Carlo (MC) methods. To achieve a close correspondence to real sea level, we use a 6^{th} order AR model where the parameters are chosen to minimize the squared forward and backward prediction error of linearly detrended GSL since 1900. This procedure guarantees that a noise realization will have a very similar spectrum to the observed GSL although the total variance and linear trend will be different. It is not necessary to simulate the low-frequency behavior of sea level (e.g. the linear trend) as we will be applying a nonlinear detrending filter to the series. The validation procedure is outlined below:

1. Create *g* as a realization of the noise process.
2. Nonlinearly detrend *g* using a 239 month wide Bartlett window.
3. Calculate the mean curve of detrended *g* surrounding 5 volcanoes (as in fig4).
4. Make a BS estimate of the standard error on the mean curve using a thousand BS samples. Each BS sample uses 5 substitutes for the volcano dates when selecting the 12 year blocks used in the mean curve.

5. Make a BS estimate of the difference between means of the before and rise windows (again using 1 000 BS samples).
6. Repeat steps 1-5 a thousand times to allow us to estimate the empirical CDF of the standard errors for different random realizations.
7. Make MC estimates of the two standard errors to high precision from 50 000 nonlinearly detrended surrogate realizations of the noise process.
8. Compare the CDF of the BS error estimates to the corresponding MC estimates.

The results of the comparison procedure are shown in Supplementary Figure 7. We see that the BS estimates are very close to the MC estimate (less than 10% error in the BS estimate).

The true GSL record has a volcanic signal superimposed on the noise. We may therefore ask what effect it has if there is a volcanic signal added to the noise the realizations from which we base our BS estimate. This can be achieved by adding a signal to the noise generated in step 1. We specify the signal of a volcanic eruption to be

$$s(t) = \begin{cases} ct\,\mathrm{e}^{t} & t > 0 \\ 0 & t \le 0 \end{cases}$$

where t is the time in years relative to the eruption and c is a constant. The constant c is chosen so that $\max(s(t))=2\sigma$, where σ^2 is the process variance of the noise. The signal we add to step 1 is comprised of 5 such peaks. The BS error estimates are shown in Supplementary Figure 8. As expected any volcanic signal introduces a positive bias in the BS error estimates. We therefore conclude that the BS error estimates are conservative.

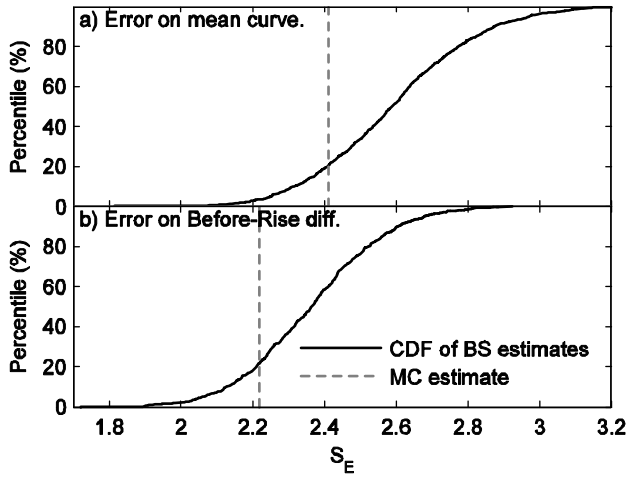

Supplementary Figure 8: Same as Supplementary Figure 7 but for the case where there is a small volcanic signal on the BS realizations.

Supplementary Methods 4: Volcanic eruptions used.

In Supplementary Table 2 we list the 10 largest eruptions since 1890 that caused at least ~10% of the Pinatubo 1991 radiative forcing (30). Other well known eruptions such as Mount St. Helens 1980 and Bezymianny 1956 had little effect on stratospheric optical depth (30). The stratospheric aerosol loading from volcanic eruptions appear to be log-normally distributed with many more eruptions causing optical depths in the range from 0-0.05 than from 0.05-0.10. The average impact of all eruptions will therefore be dominated by the smallest, which will produce smaller changes in GSL than many other factors. Very few eruptions had stratospheric aerosol loadings comparable to the 3 largest (Agung 1963, El Chichón 1982, Pinatubo 1991) and we therefore primarily use only the major 5 eruptions that caused the largest global average stratospheric optical depth (see Supplementary Table 2). Including more eruptions also increases the chance that the period surrounding an eruption was influenced by other eruptions of similar magnitude, thus obscuring the impact. All 5 volcanoes are located in the tropics and their eruption aerosol spread globally causing a significant dimming in both hemispheres (30, 5). Although the Fernandina 1968 and Colima 1890 eruptions had very similar impacts on stratospheric aerosol optical depth, and both pre-eruption periods were affected by earlier eruptions, we include only Colima 1890 to facilitate a more direct comparison with the study of Church et al. (2). However, we note that the results are robust against including Fernandina 1968.

Supplementary Table 2: Eruptions considered in this study. The stratospheric aerosol optical depths listed are the maximum at 550 nm in the 3 years following the eruption date (30).

Eruption (31)	Global Optical depth (30)	SH Optical depth (30)	Latitude, Longitude	Comment
Colima, Feb. 1890	0.048	0.043	20°N, 104°W	Tropical. Pre-eruption period likely affected by several other eruptions.
Thompson Island, 1896	0.028	0.056	54°S, 6°E ?	Not included. Existence doubtful (31).
Santa Maria, Oct. 1902	0.082	0.081	15°N, 92°W	Tropical.
Novarupta/Katmai, Jun.1912	0.040	0.000	58°N, 155°W	
Manam, Aug. 1919	0.017	0.017	4°S, 145°E	Tropical.
Agung, Mar. 1963	0.088	0.141	8°N, 116°E	Tropical.
Fernandina, Jun. 1968	0.047	0.046	0°N, 92°W	Tropical. Pre-eruption period likely affected by Agung 1963.
Fuego, Oct. 1974	0.040	0.040	14°N, 91°W	Tropical.
El Chichón, Apr. 1982	0.098	0.062	17°N, 93°W	Tropical.
Pinatubo, Jun.1991	0.149	0.148	15°N, 120°E	Tropical.

We present an alternative method of calculating the impact of volcanic eruptions on GSL based on the average impact of all 9 largest eruptions since 1890 (listed in Supplementary Table 2). We produce a mean GSL curve around the eruption date by weighting each GSL response by the maximum global stratospheric optical depth (see Supplementary Table 2) of its corresponding eruption. This weighting was chosen so that the smallest eruptions do not dominate the average. As for the 5 major tropical eruptions, we observe a clear rise in sea level in the year following an eruption (see Supplementary Figure 9). The Before to Rise window mean difference (5.4±2.6 mm) and the Rise to Drop window mean difference (6.2±3.2mm) are both significant at the 95% confidence level. However, the drop attributed to lower GOHC does not appear significantly different from zero. The magnitude of the drop is larger if the 9 eruptions are weighted by Southern Hemisphere (SH) stratospheric aerosol optical depth. This observation is consistent with the larger ocean fraction, and hence greater impact on GOHC of increased optical depth in the Southern Hemisphere.

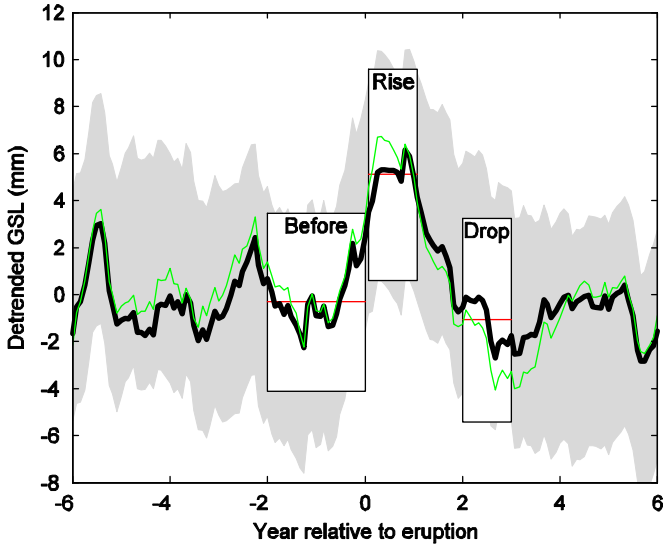

Supplementary Figure 9: Average impact of 9 major volcanoes on sea level weighted by global average stratospheric optical depth. The solid thick black curve shows non-linearly detrended GSL (10 year lag) as observed in tide gauge records (grey band show the 95% confidence interval). Boxes show the mean sea level (centre line of box) of the “Before”, “Rise” and “Drop” windows with top and bottom edges showing the 95% confidence interval of the window mean. Thin green line shows detrended GSL (10 year lag), but weighted by Southern Hemisphere stratospheric aerosol optical depth (30).

The Santa Maria 1902 eruption is the largest contributor to the rise in sea level in Figure 4. Here we calculate the average impact excluding this eruption as a sensitivity test. The resulting mean impact of the remaining 4 eruptions is shown in Supplementary Figure 10. Qualitatively the impact remains the same (peak followed by drop) and we conclude that the results robust to arbitrarily excluding Santa Maria 1902. The significance of the rise and drop in Supplementary Figure 10 is discussed in the main paper.

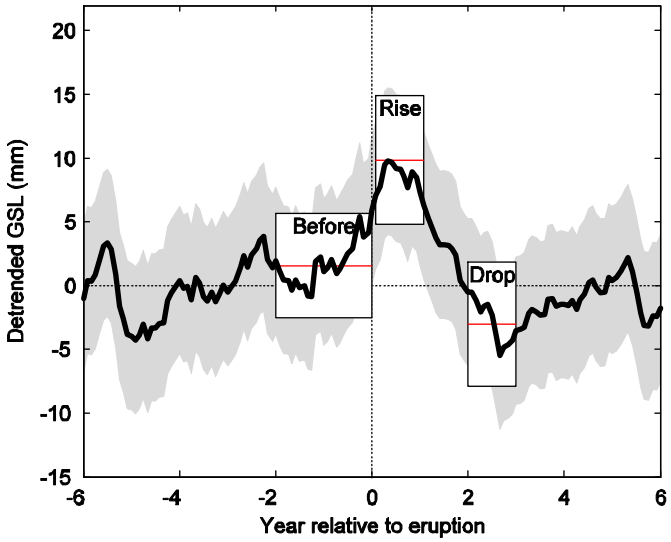

Supplementary Figure 10: Average impact of 4 major volcanoes (same as in Figure 2 excluding the 1902 Santa Maria eruption) on sea level. The solid thick black curve shows non-linearly detrended GSL (10 year lag) as observed in tide gauge records (grey band show the 95% confidence interval). Boxes show the median sea level (centre line of box) of the "Before", "Rise" and "Drop" windows. Top and bottom edges show the 95% confidence interval of the median.

Supplementary Methods 5: Differences of the present GSL reconstruction to the Jevrejeva et al. (2006) reconstruction.

Although we used the virtual station method to reconstruct global sea level in *Jevrejeva et al.* (9) there are several small differences to the reconstruction used in this study. It is important to realize that the time scales that the two studies focus on are very different. In particular the GSL reconstruction in the present study focuses on high frequency variability and in turn makes sacrifices that may influence long term trends. A comparison between the two reconstructions can be seen in Supplementary Figure 11. In *Jevrejeva et al.* (9) we chose not to apply an inverse barometer correction because historical data are limited back in time. However, volcanic eruptions can also cause large-scale shifts in atmospheric pressure patterns (see main paper). To minimize the direct impact of such shifts on sea level it is necessary to apply an inverse barometer correction.

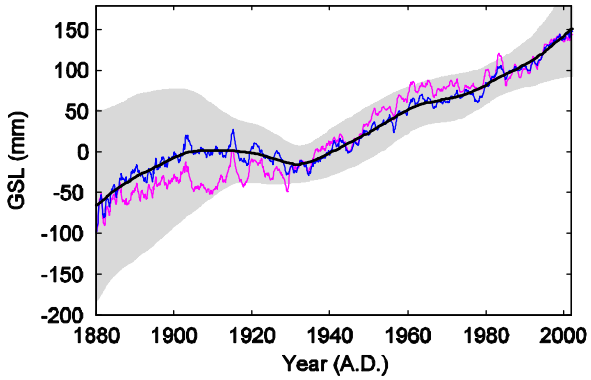

Supplementary Figure 11: GSL relative to the 20th century mean. A comparison of the reconstruction of this study (blue) and the reconstruction of *Jevrejeva et al.* (9) (magenta). The non-linear trend (10 year lag) of the present GSL reconstruction and its 2σ confidence interval (a region based jack-knife estimate) is shown as black and a grey shaded area.

The largest source of differences between the two reconstructions lie in the different set of GIA corrections applied. This is particularly evident in the period from 1885 to 1935 in Supplementary Figure 11 where there are large differences in the average GIAs used for the Arctic, N.E. Pacific and Indian regions (and Baltic). In *Jevrejeva et al.* (9) we used the *Peltier* (32) 2001 GIA corrections because they gave more consistent results across different regions. In the present study we use the corrections of *Peltier*(26) from 2004, as they are more complete, not because we consider them better than the earlier GIA corrections. The GIA corrections, however, only affects the long term trends and hence, the choice does not change any of our conclusions.

In *Jevrejeva et al.* (9) we removed all Japanese tide gauges from the analysis because of uncertainties with earthquake related vertical land movement. In the present study we instead deal with this problem statistically by removing outlier rates and stations with a highly skewed rate distribution. A summary of the differences between the GSL reconstruction of this study and the *Jevrejeva et al.* (9) reconstruction can be found in Supplementary Table 3.

Supplementary Table 3: Differences between the GSL reconstruction of this study to the reconstruction of *Jevrejeva et al.* (9) (2006).

Difference	**Jevrejeva et al. (9) (2006)**	**Present study**
Pressure correction	None	HADSLP2
Japanese tide gauges excluded	Yes	No
Outlier rate removal	No	Yes
Removal of stations that have sea level rates with skewness>0.8	No	Yes
GIA correction	*Peltier* (32) (2001)	*Peltier* (26) (2004)

Supplementary Methods 6: Comparison with the Church and White (2006) reconstruction.

Church and White (5) reconstructed global mean sea level (see Figure 3) using a variant of the optimal interpolation scheme by *Kaplan et al.* (33). The leading Empirical Orthogonal Functions (EOFs) were determined from 12 years (1993-2004) of detrended TOPEX/Poseidon and Jason-1 satellite altimeter data. The Principal Components of the leading EOFs were then determined in a least squares manner to fit the tide gauge observations. Details of the method can be found in *Church and White* (5) and *Church et al.* (4).

We note that the last 12 years have been exceptionally warm compared with the historical records (27, 28) and that the EOF patterns may not be representative of the patterns that prevailed earlier in the century. Our virtual station method does not have this global warming bias as it is completely independent of the recent satellite altimetry data. Further, *Kaplan et al.* (33*)* caution against using too short a time period for calculating the EOFs: "As emphasized in K98, reliable estimation of the space covariance matrix is the most crucial element of our method. To obtain faithful field reconstructions, we have to use a relatively long time period for the covariance estimation, and there should be enough data in it for estimating all necessary cross covariances." (here K98 refers to an earlier study). *Kaplan et al.* (33) use the period 1951-1992 for their analysis. *Church and White* (5) do acknowledge problems in the early part of their reconstruction: "Variability in GMSL trends prior to 1930 are not significant." For these reasons we consider our virtual station estimate less biased and especially so for the pre-1950 period.

Church et al. (2) modeled drops in ocean heat content and consequently sea level following major volcanic eruptions. They assert that "These post-eruption drops in sea level agree qualitatively with the observed (tide-gauge based[§]) GMSL record." Here [§] refers to the Global Mean Sea Level (GMSL) reconstruction of *Church et al.* (*4*), which as we have noted is dependent on satellite altimetry. This study has since been updated with more satellite and tide gauge data in *Church and White* (5). In *Church and White* (5) the qualitative evidence of a deceleration in GMSL following eruptions is summarized: "The post-1960 major volcanic eruptions of Mt. Agung (1963), El Chichon (1982) and Mt Pinatubo (1991) offset about 0.005 mm/yr^2 of the acceleration that is otherwise present, perhaps explaining why little acceleration has been detected over the second half of the 20th century." In Supplementary Figure 12 we examine the average impact of 5 volcanic eruptions on the detrended GMSL reconstruction by *Church and White* (5), following the same procedure used for our virtual station reconstruction. The window location of the 'Drop' boxplot was chosen to match the modeled drop in GOHC seen after Pinatubo (2). We find that the medians of the two boxes are only significantly different at the 65% confidence level (see method in main paper). Moving the 'Drop' window further away from the 'Before' window does not improve the significance. We therefore conclude that the predicted drop in sea level does not appear significant for these 5 volcanoes using the *Church and White* (5) reconstruction.

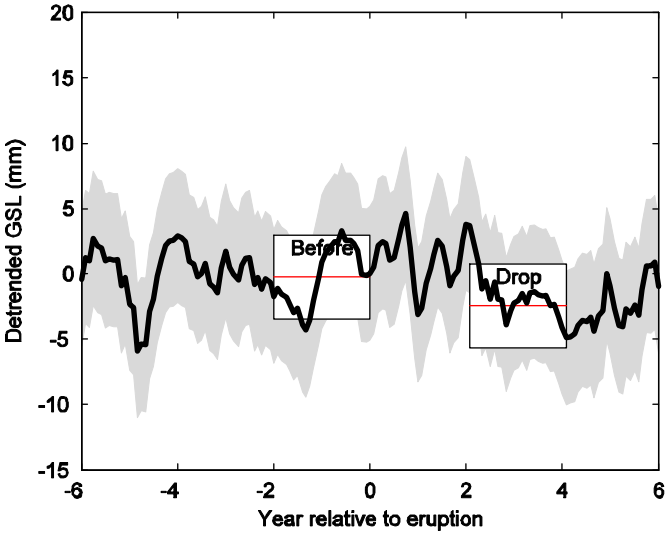

Supplementary Figure 12: Average impact of 5 major volcanic eruptions (solid black) on the detrended GMSL reconstruction of *Church and White* (5). Shaded area shows 95% confidence interval.

Supplementary Methods 7: Is the observed response dominated by ENSO variability?

Several of the large eruptions used in this study occurred during El Niño events. Perhaps El Niño prevailed slightly more often than the expectation value for the 5 volcanoes in our study. We may therefore ask if the apparent average volcanic response in figure 4 is really caused by residual ENSO variability. We note that our bootstrap confidence intervals take this into account by design. In this section we show that our conclusions are robust against removing ENSO variability from GSL prior to analysis.

Here we repeat the calculation of the volcanic impact shown in figure 4 except we remove ENSO variability prior to analysis. We remove ENSO by making a linear regression of the Niño3 index onto GSL and repeating the analysis on the residuals. We use the Niño3 index from *Kaplan et al.* (35) for the period 1856-1949 and one calculated from the SST fields from *Reynolds et al.* (36) for the period 1950-now. The removal of ENSO variability reduces the magnitude of the impact, but not significantly (see Supplementary Figure 13).

The timing of volcanic eruptions are unaffected by the phase of the ENSO. Some eruptions will by chance occur in El Niño years. In contrast, it is plausible that an eruption would have some impact on the ENSO system. E.g. perhaps the cooling weakens the trade winds (a weakening being a precursor to El Niño events). We do not argue that volcanic eruptions trigger El Niño events, rather we argue that it is important to not exclude the possibility of a volcanic influence on the ENSO system. We therefore consider the results presented in figure 4 to be more correct than those presented in this section.

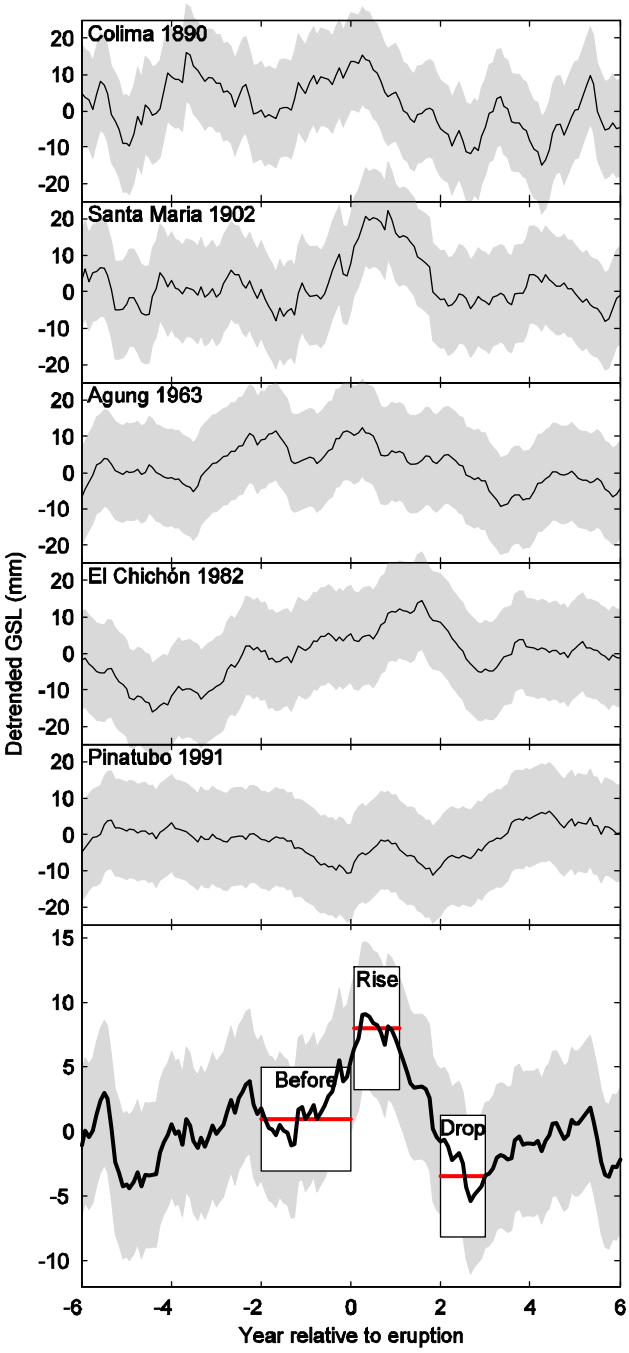

Supplementary Figure 13: The volcanic impact of 5 volcanic eruptions on detrended GSL after removing the effects of ENSO. Bottom panel shows average impact.

Key statistics:

Median(Before)-Median(Drop): 4.4±3.3mm (sig= 83%)
Median(Rise)-Median(Before): 7.0±2.8mm (sig= 98%)
Median(Rise)-Median(Drop): 11.4±3.3mm (sig>99.99%)

Supplementary Methods 8: Is the observed response dominated by solar variability?

Several of the eruptions (Colima, Santa Maria, and Agung) occur close to minima in the decadal solar cycle (1889, 1902, and 1964.9 respectively). Solar climate links have been proposed (37,38) and we may therefore ask if the solar cycle can be excluded as an explanation for the observed volcanic response in GSL. We note that the detrending filter we apply will reduce variability on 11 year periods by roughly 6dB and our results are therefore largely insensitive to a manifestation of the solar cycle in GSL. In Supplementary Figure 14 we show the wavelet coherence (39) between GSL and the International Sunspot Number (40). The very small 'significant' region at decadal periods near 1940 is most likely spurious as the relative phase relationship is completely different from 1900. We therefore conclude that it is very questionable whether there is any effect of the solar cycle on GSL at periods shorter than 20 years.

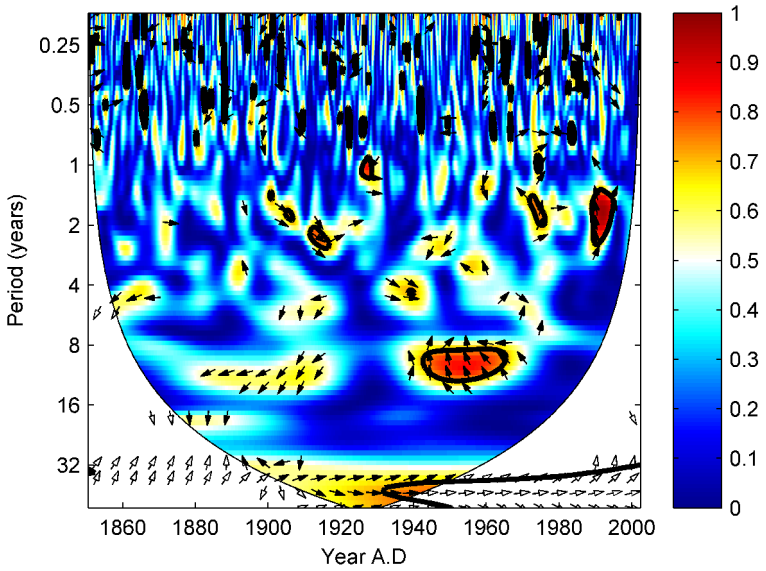

Supplementary Figure 14: Wavelet coherence between GSL and International sunspot number. Thick black contour show the 95% confidence level (tested against AR1 noise); white screening shows the 'cone of influence' where edge effects influence the results. Arrows indicate the instantaneous phase relationship between the series at a given wavelength (arrows pointing right: in-phase; left: anti-phase; down: GSL leading sunspots by 90°).

Supplementary Discussion: Volcanic impact on regional sea level.

Here we estimate the regional response of sea level to volcanic eruptions using the same methods we applied for the global impact (see main paper). First we calculate the sea level curve for each of the regions by integrating the regional sea level rates. However, some of the regions have missing data in the middle of its data coverage (see Figure 2) and we insert a zero sea level rate at those positions prior to integration. We then remove the non-linear trend from the regional sea level using the same SSA filter we

obtained from the GSL. We then remove all regional sea level values that had missing data in the corresponding sea level rate. The median regional sea level of the Before, Rise and Drop windows is shown in Supplementary Table 4. Uncertainties associated with the regional responses are unknown but are certainly larger than for the global response as fewer stations are available and in some regions the tide gauge data does not span all 5 eruptions (see Figure 2).

Supplementary Table 4: Volcanic impact on sea level in each of the regions.

Region	**Before (mm)**	**Rise (mm)**	**Drop (mm)**
Antarctic	11	-14	2
Arctic	13	27	-8
Baltic	20	47	-23
CPacific	3	-9	-17
Indian	2	0	-7
Mediterr	2	-10	-9
NEAtlantic	1	12	-10
NEPacific	-5	41	3
NWAtlantic	-2	14	-12
SEAtlantic	0	-2	3
SEPacific	-9	41	9
SWAtlantic	3	-4	33
WPacific	-3	-9	0

References.

30. M. Sato et al, *J. Geophys. Res.* **98**, 22,987–22,994 (1993).
31. L. Siebert, T. Simkin, *Volcanoes of the World: an Illustrated Catalog of Holocene Volcanoes and their Eruptions.* Smithsonian Institution, Global Volcanism Program Digital Information Series, GVP-3, (http://www.volcano.si.edu/world/), June 2006.
32. W.R. Peltier, In *Sea Level Rise* (Academic Press , Douglas, B.C., Kearney, M.S., and S.P. Leatherman, eds., 2001).
33. A. Kaplan, Y. Kushnir, M.A. Cane, *J. Clim.* **13**, 2987–3002 (2000).
34. A. M. Zoubir, D. R. Iskander, *I.S.P.M.,* **24**(4), 10-19 (2007).
35. A. Kaplan, M. Cane, Y. Kushnir, A. Clement, M. Blumenthal, B. Rajagopalan, *J. Geophys. Res.*, 103, 18,567-18,589, (1998).
36. R. W. Reynolds, N. A. Rayner, T. M. Smith, D. C. Stokes, W. Wang. *J. Climate*, 15, 1609-1625. (2002**)**
37. J. C. Moore, A. Grinsted, S. Jevrejeva, *Geophys. Res. Lett.*, 33, L17705, doi:10.1029/2006GL026501 (2006).
38. A. Grinsted, *Arctic Centre reports* 47 (2006).
39. A. Grinsted, J. C. Moore, S. Jevrejeva, *Nonlin. Proc. Geophys.*, 11, 561-566, 18-11-2004.
40. SIDC-team, *Monthly Report on the International Sunspot Number, online catalogue of the sunspot index*. (http://www.sidc.be/sunspot-data/) '1749-2007'.